Measurement Science
and Technology

100 year anniversary
Measurement Science and Technology

PURPOSE-LED
PUBLISHING™

PAPER • **OPEN ACCESS**

Temperature coefficient of resistance and thermal boundary conductance determination of ruthenium thin films by micro four-point probe

To cite this article: Braulio Beltrán-Pitarch *et al* 2024 *Meas. Sci. Technol.* **35** 066012

OPEN ACCESS
IOP Publishing
Measurement Science and Technology
Meas. Sci. Technol. **35** (2024) 066012 (9pp)
https://doi.org/10.1088/1361-6501/ad366b

Temperature coefficient of resistance and thermal boundary conductance determination of ruthenium thin films by micro four-point probe

Braulio Beltrán-Pitarch[1,2,*], Benny Guralnik[1], Kasper A Borup[3], Christoph Adelmann[4], Ole Hansen[5], Nini Pryds[2] and Dirch H Petersen[2]

[1] KLA Corporation, Diplomvej 373, DK-2800 Kgs. Lyngby, Denmark
[2] DTU Energy—Department of Energy Conversion and Storage, Technical University of Denmark, Fysikvej 310, DK-2800 Kgs Lyngby, Denmark
[3] Department of Chemistry, Aarhus University, Langelandsgade 140, DK-8000 Aarhus C, Denmark
[4] Imec, Kapeldreef 75, 3001 Leuven, Belgium
[5] DTU Nanolab—National Centre for Nano Fabrication and Characterization, Technical University of Denmark, Ørsteds Plads 347, DK-2800 Kgs Lyngby, Denmark

E-mail: Braulio.BeltranPitarch@kla-tencor.com

Received 5 December 2023, revised 14 March 2024
Accepted for publication 21 March 2024
Published 2 April 2024

Abstract

Accurate characterization of the temperature coefficient of resistance (α_{TCR}) of electrically conductive materials is pertinent for reducing self-heating in electronic devices. *In-situ* non-destructive measurements of α_{TCR} using the micro four-point probe (M4PP) technique have previously been demonstrated on platinum (Pt) thin films deposited on fused silica, assuming the thermal conductivity of the substrate as known. In this study, we expand the M4PP method to obtain the α_{TCR} on industrially relevant stacks, comprising ruthenium (Ru) thin films (3.3 nm and 5.2 nm thick) deposited on bulk silicon (Si), separated by a 90 nm SiO_2 spacer. The new M4PP methodology allows simultaneous determination of both α_{TCR} and the total thermal boundary conductance (G_{TBC}) between the metallic film and its substrate. We measured the α_{TCR} and the G_{TBC} to be 542 $\pm$ 18 ppm K^{-1} and 15.6 $\pm$ 1.3 MW $m^{-2}K^{-1}$ for 3.3 nm Ru, and 982 $\pm$ 46 ppm K^{-1} and 19.3 $\pm$ 2.3 MW $m^{-2}K^{-1}$ for 5.2 nm Ru. This is in good agreement with independent measurements of α_{TCR}. Our methodology demonstrates the potential of M4PP to characterize thermal properties of metallic thin films used in semiconductor technology.

Keywords: TCR, thermal barrier, thermal boundary resistance, equivalent thermal resistance, thermal resistivity

* Author to whom any correspondence should be addressed.

1. Introduction

The temperature coefficient of resistance (α_{TCR}) defines the fractional change in the electrical resistivity of a material due to an increase in temperature. For most metals near room temperature, α_{TCR} is positive, which entails an unwanted heating of electronic devices and sensors. Thus, to ensure device performance, α_{TCR} must be considered during their design and monitored during production to avoid losses in efficiency, performance and reliability [1–3]. In addition, α_{TCR} can be used as an indirect measure of critical dimension [4], and as an early warning indicator of thermal failure [5, 6].

The prevalent approach for measuring α_{TCR} involves recording the electrical resistivity at various steady-state temperatures, and determining the slope $\partial R/R\partial T$ through linear fitting of the experimental data [7]. Although this is a simple and effective method, it is time-consuming since it requires sample preparation and significant measurement time to allow the temperature to stabilize at several set points. Furthermore, it usually involves additional steps of sample preparation (e.g. use of conductive paint) to improve the electrical contacts. Thus, development of a method for fast and accurate measurement of α_{TCR} is highly relevant.

Micro four-point probe (M4PP) is commonly utilized for spatial characterization of material properties, to enhance process control and optimization. The M4PP technique has been extensively used for measuring sheet resistance [8, 9], electron mobility [10, 11], carrier density [10, 11], and tunneling magnetoresistance [12, 13] mainly at wafer level in semiconductor manufacturing and research.

Recently, we have demonstrated the potential of the M4PP technique to determine several thermal and thermoelectric properties. These developments include the determination of α_{TCR} of metallic thin films deposited on fused silica [14], extraction of the ratio of the Seebeck coefficient to the thermal conductivity [15], spatial probing of microscopic thermal fields [16], and measurement of thermal diffusivity [17]. Previously, we conducted α_{TCR} measurements on platinum (Pt) thin films deposited on fused silica, as documented in [14]. However, these samples do not align with standard silicon (Si) substrates widely used in semiconductor research and manufacturing. Commonly, thin-film metals are deposited on a thin SiO_2 layer (less than 500 nm) grown on a silicon wafer. M4PP measurements on such wafers present a considerable challenge due to the high thermal conductivity of the substrate, which diminishes all the temperature-dependent signals. Furthermore, the presence and influence of the SiO_2 layer are non-negligible factors that add complexity to the analytical model required to accurately derive α_{TCR}.

In this study, we present an improved method that allows the characterization of α_{TCR} even for samples with standard Si substrates. In addition, instead of using a semi-analytical model, we use the finite element method (FEM), which decreases the computational time. The new approach is demonstrated on two ruthenium (Ru) thin films deposited on 90 nm of SiO_2 grown on a Si substrate. Measurements of α_{TCR} using M4PP and a physical property measurement system (PPMS) are compared, and found to be in excellent agreement. The M4PP measurements also allow the determination of the total thermal boundary conductance between the metallic thin films and their Si substrate (G_{TBC}).

2. Theoretical model

M4PP measurements are performed on a metallic thin film by forcing an alternating current $I(t) = \sqrt{2} I_{\mathrm{RMS}} \sin(\omega t)$ at an angular frequency ω between two electrodes on a sample. Here, t is the time and I_{RMS} is the root mean square of the current. The forced current results in a potential difference $V(t)$ that is probed with two other electrodes, as represented in figure 1(a). The measurement current causes a local temperature increase at an angular frequency $2\,\omega\,\Delta T(\mathbf{r}) \propto I^2$ due to Joule heating at the location $\mathbf{r}$, as can be seen in figure 1(b). This temperature increase results in a change in the local sheet resistance $R_S(\mathbf{r})$, which for small temperature changes are well described by the linear approximation $R_S(\mathbf{r}) = R_{S,0}[1 + \alpha_{\mathrm{TCR}}\Delta T(\mathbf{r})]$, where $R_{S,0}$ is the sheet resistance at reference (room) temperature.

The resulting four-point voltage, which is represented in figure 1(c), can be described as $V(t) = R_0 I(t) + R_0 \alpha_{\mathrm{TCR}} \Psi I^3(t)$ where R_0 is the zero-current four-point resistance (without Joule heating) and Ψ is a function of material properties and geometry [18], including the thermal boundary conductance G_{TBC} between metal thin film and Si substrate. Typically, the four-point voltage is measured via lock-in amplification, and we define the first and third harmonic resistances $R_{1\omega}$ and $R_{3\omega}$ via $V(t) = \sqrt{2} I_{\mathrm{RMS}}[R_{1\omega}\sin(\omega t) + R_{3\omega}\sin(3\omega t)]$ [18]. It should be clarified that the origin of $R_{3\omega}$ is temperature fluctuating at an angular frequency 2ω, and not temperature at an angular frequency 3ω. To estimate α_{TCR}, it is convenient to measure $R_{3\omega} = -\frac{1}{2} R_0 \alpha_{\mathrm{TCR}} \Psi I_{\mathrm{RMS}}^2$ [18] as an alternative to using the resistance difference obtained from measurements at two different currents [14]. Using $R_{3\omega}$ is particularly advantageous when measuring weak signals, as is the case of samples with Si as substrate.

Figure 2 presents FEM simulations of $R_{3\omega}$ as function of pitch s in configurations A′ and A for different combinations of α_{TCR} and G_{TBC}. The use of A and A′ configurations is justified since it minimizes unwanted thermoelectric contributions [14, 15]. The insets in figure 2 show a schematic of the configurations used and the definition of pitch. It can be seen that weaker $R_{3\omega}$ signals are produced in both configurations when (i) measuring with larger electrode pitch and (ii) in A configuration compared with A′ configuration (notice the difference in scale between figures 2(a) and (b)). Furthermore, the influence of α_{TCR} and G_{TBC} on $R_{3\omega}$ depends on the pitch and the measurement configuration (see figure 2). To summarize, the simulations in figure 2 suggest that it should be possible to determine simultaneously α_{TCR} and G_{TBC} by performing two or more measurements with different configuration and/or pitch.

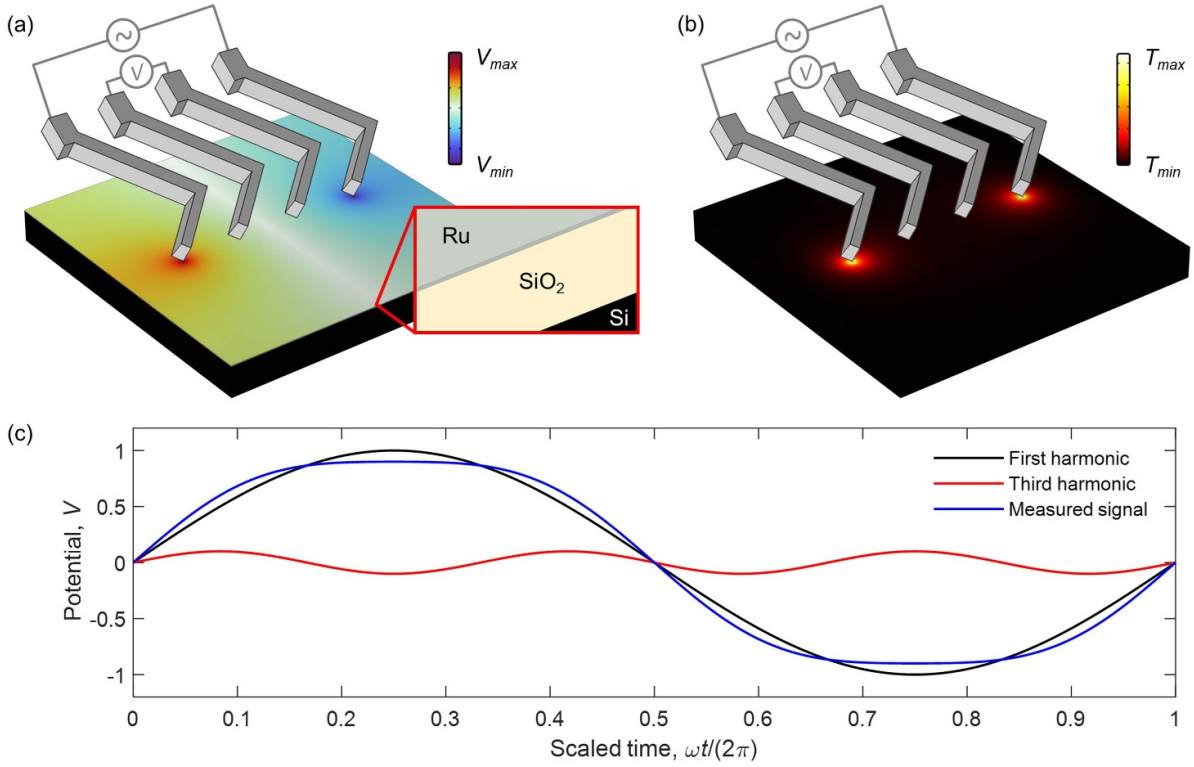

Figure 1. Schematic view of the M4PP setup on a multilayered system consisting of an electrically conductive Ru thin film deposited on SiO_2 with Si as substrate. The (a) electric potential and (b) temperature when a constant current is applied/extracted at the outer electrodes were obtained using COMSOL Multiphysics 6.1. (c) Simulated waveforms for the extreme case of $R_{3\omega}/R_{1\omega} = 0.1$, the actual experimental ratios are several orders of magnitude lower.

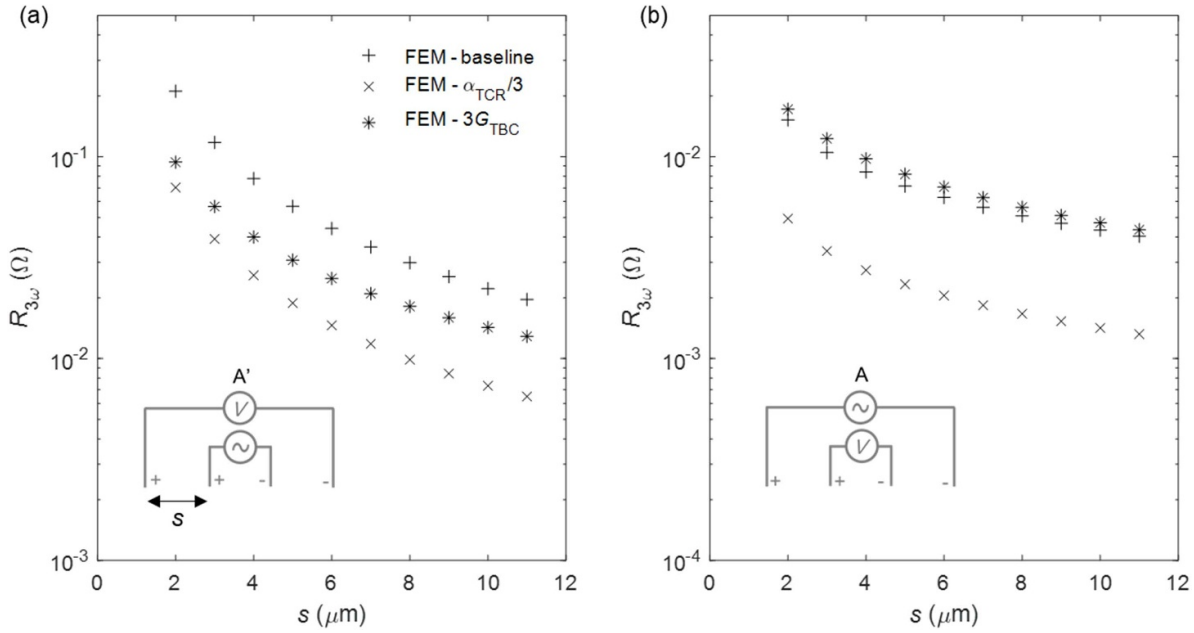

Figure 2. FEM simulations of the third harmonic resistance for different pitches in (a) A′ and (b) A configurations. Different combinations of temperature coefficient of resistance and thermal boundary conductance are plotted. All simulations were performed for a 3.3 nm Ru thin film ($R_{S,0} = 171\ \Omega$ and thermal conductivity of 12.7 W m K^{-1}) deposited on 90 nm of SiO_2 (1.5 W m K^{-1}) with Si (130 W m K^{-1}) as substrate, using $I_{RMS} = 5$ mA, $\alpha_{TCR} = 542$ ppm K^{-1}, and considering a probe contact radii of 130 nm. The inset is a schematic of the configuration used.

Table 1. Summary of the steps followed in this work to determine the temperature coefficient of resistance of a metallic thin film and the total thermal boundary conductance between the thin film and its substrate.

	Unknown parameters	Obtained from	References
1	Zero-current four-point resistance R_0	Measured $R_{1\omega}$ and $R_{3\omega}$ ($R_0 = R_{1\omega} + 3R_{3\omega}$)	[18]
2	Sheet resistance $R_{S,0}$ and accurate position of the electrodes	Multiple zero-current four-point resistance estimates R_0	[13]
3	Thermal conductivity of the metallic thin film	Wiedemann–Franz law	[19]
4	Contact radii of current electrodes	Multiple two-point resistance measurements	[15]
5	Temperature coefficient of resistance α_{TCR} and total thermal boundary conductance G_{TBC}	Fitting numerically to $R_{3\omega}$ using at least two measurements in different configuration or pitch	This work

Although a semi-analytical expression for α_{TCR} of a thin film on a bulk substrate has been derived [14], the approach is inapplicable to samples with an additional electrically-insulating yet thermally-conductive layer between the metallic thin film and the substrate, as the case with our current samples. To overcome this drawback, in the present study, we use FEM to simulate the electrical and thermal responses of the sample (see appendix A for simulation details). For data fitting, the FEM simulations were further performed with direct current $I_{DC} \equiv I_{RMS}$ to reduce execution time. Each FEM simulation provided the four-point resistance R_{DC} and the zero-current resistance $R_{DC,0}$ (by setting $\alpha_{TCR} = 0$). The misfit to experimental data for an individual measurement i is then given by,

$$\varepsilon_i = \frac{R_{3\omega,i}}{R_{0,i}} - \frac{1}{2}\frac{R_{DC,i} - R_{DC,0,i}}{R_{DC,0,i}}, \tag{1}$$

where the factor 1/2 arises from the definition $I_{DC} \equiv I_{RMS}$ [14]. Notice that in the limit of a small current, the first harmonic resistance $R_{1\omega} = R_0$ and the third harmonic term vanishes, $R_{3\omega} \approx 0$. At larger currents in the low-frequency limit, where heat transport is considered instantaneous within the measured volume, the zero-current four-point resistance can be obtained from $R_0 = R_{1\omega} + 3R_{3\omega}$ [18].

The main factors that affect $R_{3\omega}$ are: (1) $R_{S,0}$ and (2) thermal conductivity of the electrically conductive thin film, (3) electrode pitch, (4) electrode contact radii, (5) α_{TCR} and (6) G_{TBC}. The $R_{S,0}$ and the accurate position of the electrodes were calculated by regression, using R_0 from several configurations [13]. Since the top layer is metallic, its thermal conductivity was estimated using the Wiedemann–Franz law once $R_{S,0}$ was determined. Then, the contact radii of the current electrodes were calculated from the two-point load resistance of multiple configurations [15]. Finally, the remaining two parameters (α_{TCR} and G_{TBC}) were fitted simultaneously, provided measurements in A′ and A configurations for different electrode pitch. A summary of the workflow is shown in table 1.

3. Materials and instrumentation

Two Ru thin films (3.3 nm and 5.2 nm thick) were deposited by atomic layer deposition with an adhesion layer of TiN (0.3 nm) on 90 nm of SiO_2 grown on 300 mm Si (100) wafers (see inset figure in figure 1(a)). Further information about the sample preparation can be found in [20, 21]. Both samples were cut in a square shape of approximately 1 cm in edge length to facilitate reference measurements with a Quantum Design PPMS. For these measurements, the surface of each Ru thin film was contacted at four locations by thin copper wires using silver (Ag) paint. The samples were then positioned in a temperature-regulated chamber, with their electrical resistance being continuously monitored as the temperature incrementally increased from 290 K to 310 K in 5 K steps. The α_{TCR} for each sample was obtained from a linear fitting of the resistance-temperature data (see figure A1 in appendix B for further details).

M4PP measurements were performed using a modified CAPRES A301 microRSP® tool equipped with a digital lock-in amplifier [18], allowing the extraction of $R_{3\omega}$. A sinusoidal current at a low frequency (3.01 Hz) was used, and the current amplitude was stepped from $I_{RMS} = 2$ mA to $I_{RMS} = 5$ mA in all measurements. The use of current steps enables to monitor the linearity of $R_{3\omega}$ with current squared and eventually can be used to reduce measurement error. The M4PP used had eight equidistant collinear electrodes with a separation of 4 μm so that it was possible to perform equidistant four-point measurements with a pitch of $s = 4$ μm and $s = 8$ μm at each probe engage with the thin-film surface. All measurements were performed at atmospheric pressure and at room temperature.

4. Results and discussion

The measured $R_{3\omega}$ in a representative engage as function of current in configurations A′ and A and pitches $s = 4$ μm and $s = 8$ μm are shown in figure 3. Current sweeps from 2 mA to 5 mA exhibited strong linearity of $R_{3\omega}$ with ${I_{RMS}}^2$, and were easily reproducible for all the four combinations of pitch and configuration by the FEM model using a single pair of (α_{TCR}, G_{TBC}). In order to reduce measurement error, the individual data of each current sweep was fitted using $R_{3\omega} = a{I_{RMS}}^2$ to obtain a current-independent slope a; the FEM model sought to reproduce only this slope (and not the entire dataset), as realized at an arbitrary $I_{RMS} = 5$ mA. Such a treatment resulted in largely indistinguishable estimates of α_{TCR} and G_{TBC}

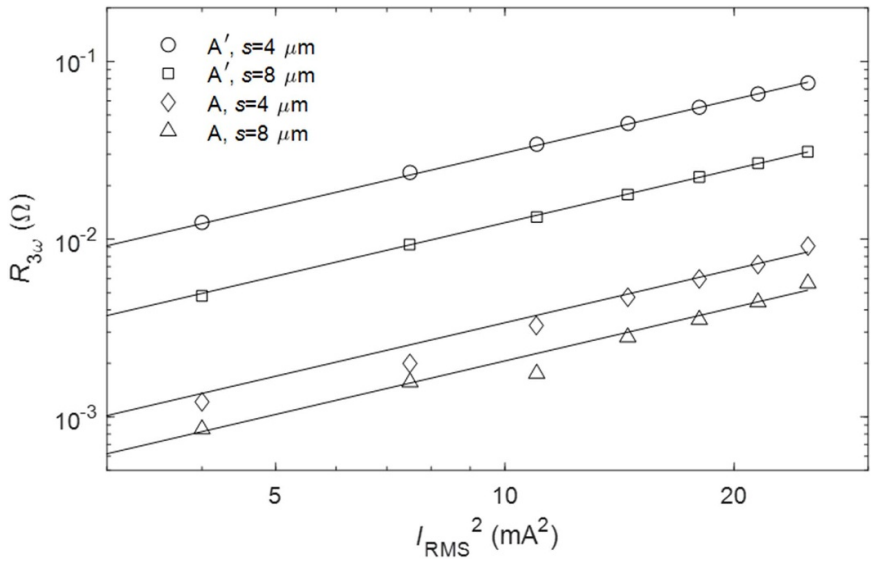

Figure 3. The empty symbols represent the measured third harmonic resistance at different currents for a single engage of the 3.3 nm Ru thin film, while the lines show their respective best fits using $R_{3\omega} = aI_{\mathrm{RMS}}{}^2$.

(as compared to the fitting of all data points), but further reduced their scatter, while also considerably decreasing the FEM runtime by about a tenfold.

The parameters α_{TCR} and G_{TBC} were fitted simultaneously in COMSOL Multiphysics 6.1 with MATLAB to the four slopes (represented by $R_{3\omega}$ values regressed at $I_{\mathrm{RMS}} = 5$ mA), by minimizing the total misfit, $\varepsilon_T = \sum \varepsilon_i$, where i represents each of the four independent measurements, and ε_i is given by equation (1). Figure 4 shows the best-fit values of α_{TCR} and G_{TBC} with their respective uncertainties for 30 probe engages with a step size of 1 μm (color symbols), alongside the independent reference measurements of α_{TCR} performed by PPMS (dashed lines in figure 4(a)), and the expected intrinsic specific thermal conductance of the SiO_2 layer alone (dashed line in figure 4(b)), considering a thickness of 90 nm and thermal conductivity of 1.33 W m K^{-1} [22]. All engages were treated independently, and they did not consider thermoelectric effects (see appendix C for proof of this contribution being negligible). The means of the best-fitted α_{TCR} and G_{TBC} were 542 ± 18 ppm K^{-1} and 15.6 ± 1.3 MW m^{-2} K^{-1} for the 3.3 nm Ru thin film, and 982 ± 46 ppm K^{-1} and 19.3 ± 2.3 MW m^{-2} K^{-1} for the 5.2 nm Ru thin film. Although the microstructure of the thin films may affect the variation of α_{TCR} with thickness in different ways [23], a lower α_{TCR} for thinner thin films could be explained due to additional scattering processes at the surfaces of the film. In brief, when temperature increases, the mean free path of electrons decreases, reducing the relative contribution of the surface scattering to the phonon scattering [24].

The mean α_{TCR} of the thinnest Ru sample is ≈9% lower than the PPMS reference value, although the reason could be an overestimation of the electrical resistance measured by PPMS due to the use of Ag paint [25]. The mean α_{TCR} of the 5.2 nm Ru thin film is ≈5% larger than the reference measurement, and most probe engages (≈2/3) overlap with the PPMS value when the fitting uncertainty is considered. Assuming the thermal boundary conductance is purely determined by the SiO_2 layer (neglecting the thermal interface resistances), the mean G_{TBC} value obtained for the 3.3 nm Ru thin film corresponds to a SiO_2 thermal conductivity of 1.40 ± 0.12 W m K^{-1}. The thermal conductivity was calculated as $\kappa_{\mathrm{SiO2}} = G_{\mathrm{TBC}} h_{\mathrm{SiO2}}$, where κ_{SiO2} and h_{SiO2} are the thermal conductivity and thickness (90 nm) of the SiO_2 layer, respectively. This compares well with the intrinsic thermal conductivity of thin SiO_2, 1.33 W m K^{-1} [22], indicating a negligible influence of the interface resistances. G_{TBC} extracted from the 5.2 nm Ru thin film results in a thermal conductivity of 1.74 ± 0.21 W m K^{-1}. This value is unexpectedly larger than the 3.3 nm Ru thin film (since the thickness of the SiO_2 layer is the same in both samples), and the reason could be an overestimation of the contact radii, which mainly depends on the calibration measurement [15]. The calibration measurement has a stronger influence on thicker thin films due to their lower sheet resistance ($R_{S,0} \approx 170\ \Omega$ and $R_{S,0} \approx 60\ \Omega$ for the 3.3 nm and 5.2 nm Ru thin films, respectively). The fitting uncertainty of both parameters (α_{TCR} and G_{TBC}) is also systematically larger for the 5.2 nm thin film, which is likely due to weaker $R_{3\omega}$ signals also produced by the lower $R_{S,0}$ of this thin film.

Finally, a sensitivity analysis in the form of Monte Carlo simulations was performed for both thin films as can be seen in figure 5. First, a FEM simulation for each sample was computed for the same pitches ($s = 4$ μm and $s = 8$ μm), configurations (A′ and A) and current ($I_{\mathrm{RMS}} = 5$ mA) as the experimental measurements. For the 3.3 nm Ru thin film $R_{S,0} = 170\ \Omega$, $\alpha_{\mathrm{TCR}} = 550$ ppm K^{-1}, and a thermal conductivity of 12.7 W m K^{-1}, while for the 5.2 nm Ru thin film $R_{S,0} = 60\ \Omega$, $\alpha_{\mathrm{TCR}} = 950$ ppm K^{-1}, and a thermal conductivity

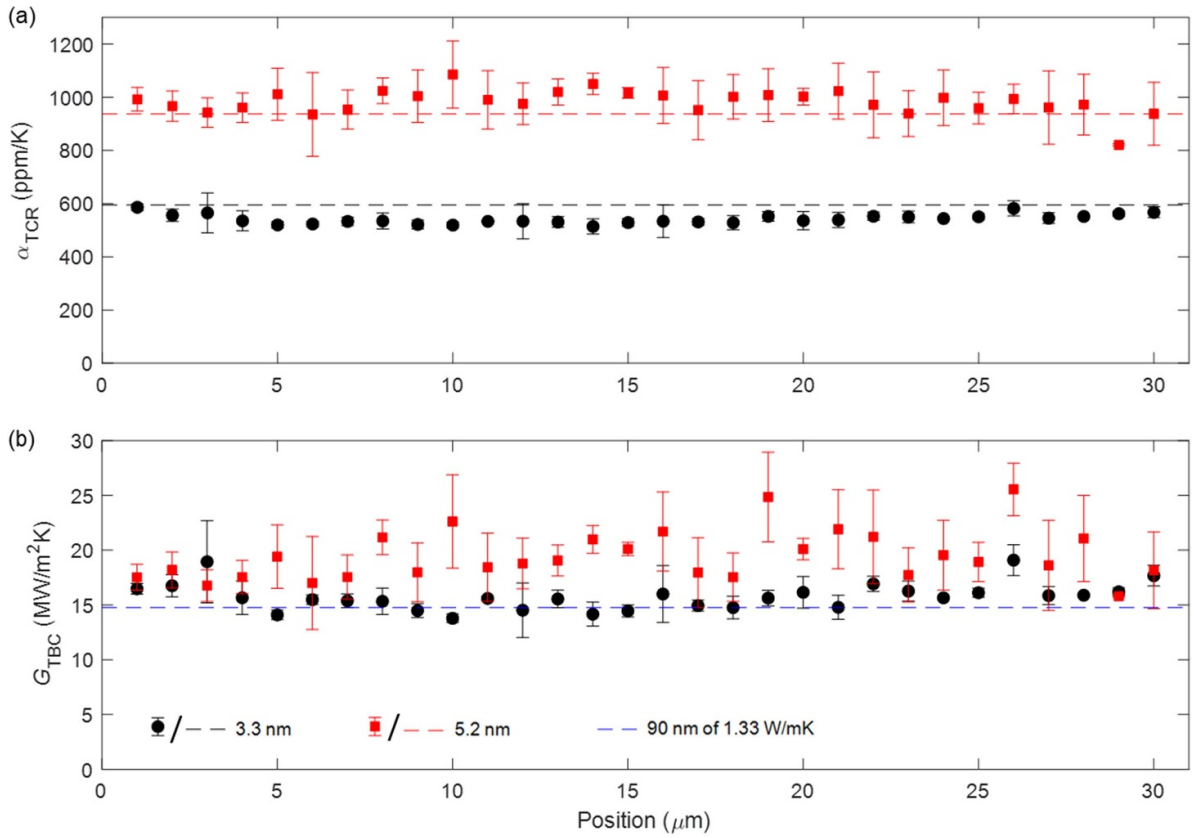

Figure 4. (a) Temperature coefficient of resistance of the Ru thin films and (b) total thermal boundary conductance between the Ru and its Si substrate with their respective fitting errors for the two samples studied in this work. The dashed lines in (a) indicate the reference values given by PPMS, while the dashed line in (b) represents the intrinsic specific thermal conductance of 90 nm of a material with a thermal conductivity of 1.33 W m K^{-1}.

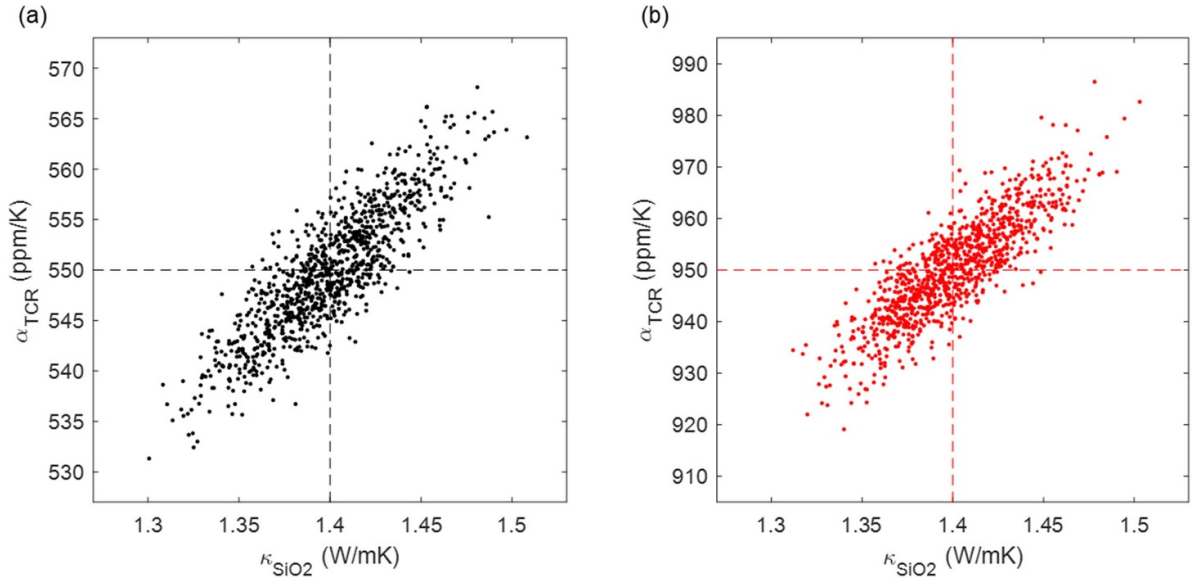

Figure 5. Output of the Monte Carlo simulations for the (a) 3.3 Ru and (b) 5.2 Ru thin films. For each thin film, 1000 independent fittings to artificially generated data with 1% normally distributed electrical noise in $R_{3\omega}$ were performed. All fittings were executed at the same pitches and configurations as measured experimentally ($s = 4$ μm and $s = 8$ μm in A′ and A). The 3.3 nm Ru thin film ($R_{S,0} = 170$ Ω, $\alpha_{TCR} = 550$ ppm K^{-1}, and thermal conductivity of 12.7 W m K^{-1}) and the 5.2 Ru thin film ($R_{S,0} = 60$ Ω, $\alpha_{TCR} = 950$ ppm K^{-1}, and thermal conductivity of 22.9 W m K^{-1}) were considered in perfect contact with the 90 nm of SiO_2 (1.4 W m K^{-1}) on the Si substrate (130 W m K^{-1}). A current $I_{RMS} = 5$ mA, and a probe contact radii of 130 nm were used.

of 22.9 W m K^{-1} were used. The remaining parameters were identical for both samples and similar to the expected values (90 nm of $\kappa_{SiO2} = 1.4$ W m K^{-1} for the SiO_2 layer with negligible thermal interface resistances, a thermal conductivity of 130 W m K^{-1} for the Si substrate, and a probe contact radii of 130 nm). The simulations provided four values of $R_{3\omega}$ for each thin film (corresponding to all combinations of the 2 pitches and the 2 configurations). Then, a set of 1000 independent measurements were artificially generated by adding a normally distributed electrical noise with a standard deviation of 1% on the $R_{3\omega}$ values. Each of the 1000 artificial measurements (consisting of 4 values of $R_{3\omega}$) were numerically fitted to obtain simultaneously α_{TCR} and κ_{SiO2}, as shown in figure 5. As expected, the mean values of α_{TCR} were 550 ppm K^{-1} and 950 ppm K^{-1} for the 3.3 nm and 5.2 nm Ru thin films, respectively, while the mean value of κ_{SiO2} was 1.4 W m K^{-1} in both cases. The standard deviation of the fitted values for both samples was 1.1% for α_{TCR} and 2.3% for κ_{SiO2}, indicating a significantly higher sensitivity of the method for determining α_{TCR} compared to G_{TBC}, which is in agreement with the experimental data. Figure 5 also shows a stronger covariation between α_{TCR} and G_{TBC} than experimentally observed, and a possible reason could be an experimental covariation between the electrical noise of different configurations during the same engage. It also seems that the experimental electrical noise is lower than the 1% simulated.

5. Conclusions

By performing M4PP measurements with different electrode configurations and pitch, the α_{TCR} and the G_{TBC} were determined simultaneously. Here, we have characterized two Ru thin films (3.3 nm and 5.2 nm thick) on 90 nm of SiO_2 deposited on Si. The system was modeled using the FEM (COMSOL Multiphysics 6.1). The α_{TCR} and the G_{TBC} mean values obtained for 30 independent measurements on each sample were 542 ± 18 ppm K^{-1} and 15.6 ± 1.3 MW m^{-2} K^{-1} for the 3.3 nm Ru thin film as well as 982 ± 46 ppm K^{-1} and 19.3 ± 2.3 MW m^{-2} K^{-1} for the 5.2 nm Ru thin film. The mean G_{TBC} of the thinnest sample, assumed to be the most accurate, corresponds to a SiO_2 thermal conductivity of 1.40 ± 0.12 W m K^{-1}. The values of the α_{TCR} were found to be in good agreement with a PPMS, while the G_{TBC} values also agreed with literature. This study shows the potential of M4PP as a powerful tool to perform local, fast, accurate α_{TCR} and G_{TBC} measurements of metallic thin films in multilayered stacks. By optimal choice of a metallic thin film with large sheet resistance and α_{TCR}, this new M4PP method can be optimized for accurate evaluation of the effective thermal conductivity of individual layers in a multilayered stack.

Data availability statement

All data that support the findings of this study are included within the article (and any supplementary files).

Acknowledgments

The authors acknowledge financial support from Innovation Fund Denmark for the Industrial Postdoc 1045-00029B and the Independent Research Fund Denmark (Grant No. 8048-00088B).

Appendix A

All M4PP simulations were generated with COMSOL Multiphysics 6.1 using three modules: electric current in shells, heat transfer in shells, and heat transfer in solids. Only the top layer (Ru thin film) was set as electrically conductive (see figure 1), with electrical insulation at all the edges defining its perimeter, and an initial voltage of 0 V. The entire geometry was thermally conductive, with thermal insulation at the probe plane and fixed temperature (293.15 K) at all the remaining outer surfaces. The thermal conductivity of the Si substrate was provided as constant (130 W m K^{-1}) since it is not a critical parameter. Two multiphysics modules were used: electromagnetic heating (to include the Joule effect), and thermal connection (to couple the thin film layers with the substrate). Normal current density was applied/extracted through two circles at the top surface while two point probes were used to record the voltage difference (simulating the probe). Convergence tests were performed to verify that the domain size and mesh were adequate.

Appendix B

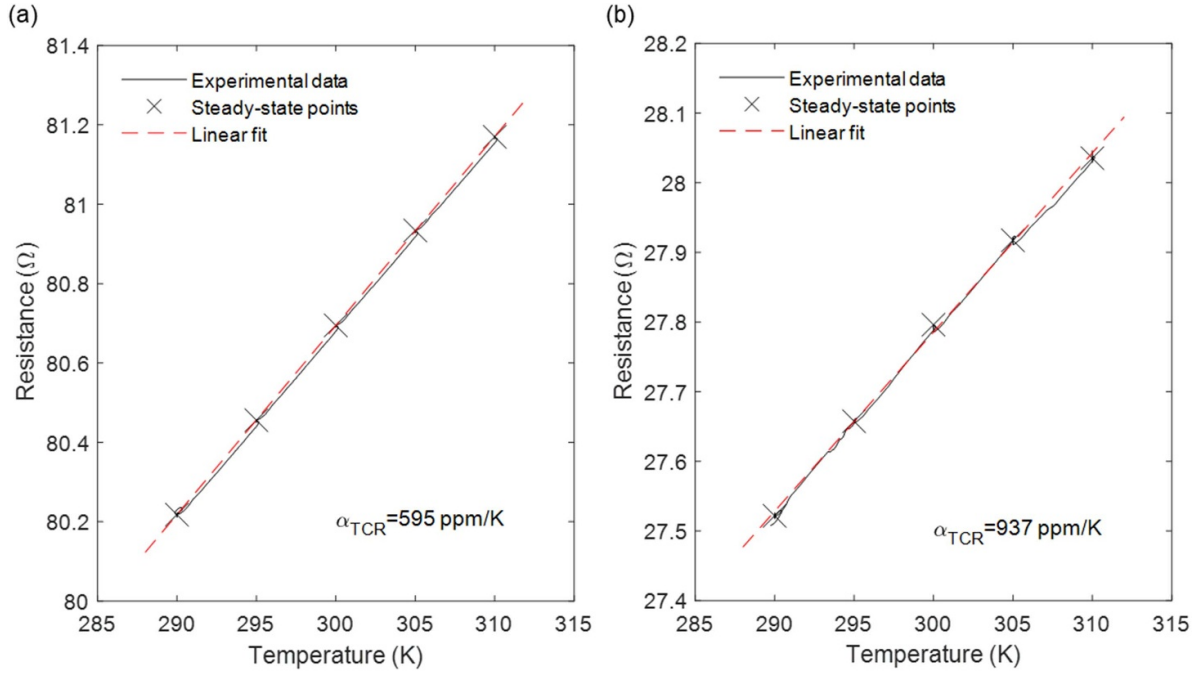

Figure A1. Temperature coefficient of resistance of the (a) 3.3 nm and (b) 5.2 nm Ru thin films measured by PPMS. The black lines show the continuous monitoring of the resistance, the crosses indicate the five steady-state points used for the fittings, and the red dashed lines represent the best fits using a linear equation. The values in the inset were extracted as $\alpha_{TCR} = \Delta R/R\Delta T$.

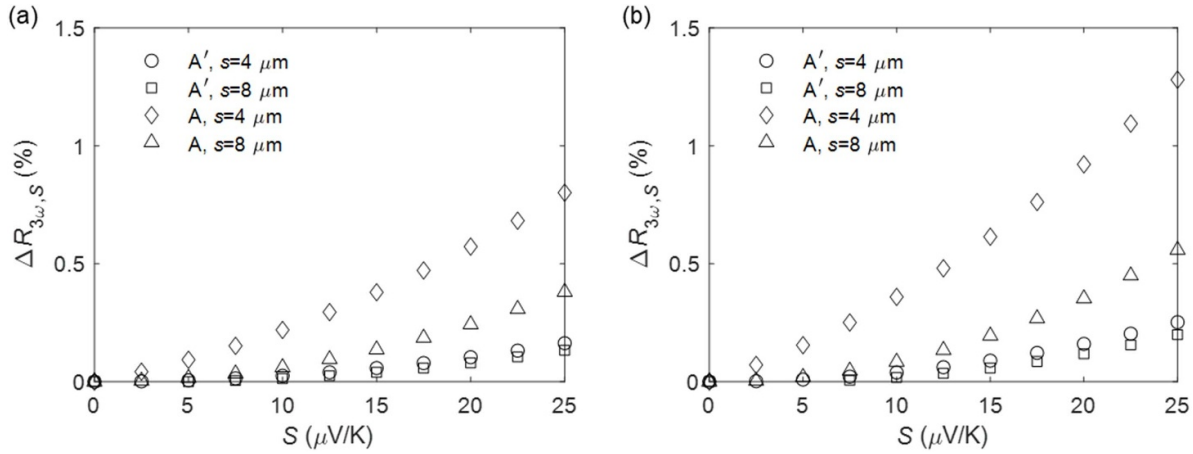

Figure A2. Increase in $R_{3\omega}$ when a difference in Seebeck coefficient between sample and probe is considered for the (a) 3.3 nm ($R_{S,0} = 171\ \Omega$, thermal conductivity of 12.7 W m K^{-1} and $\alpha_{TCR} = 542$ ppm K^{-1}) and (b) 5.2 nm ($R_{S,0} = 60\ \Omega$, thermal conductivity of 22.9 W m K^{-1} and $\alpha_{TCR} = 900$ ppm K^{-1}) Ru thin films. The simulations were generated for 90 nm of SiO_2 (1.5 W m K^{-1}) on Si (130 W m K^{-1}) under the thin films, a probe contact radii of 130 nm and an $I_{RMS} = 5$ mA.

Appendix C

To demonstrate that the thermoelectric contribution is negligible, the increase in $R_{3\omega}$ when there is a difference between the Seebeck coefficient of the sample S_S and the probe S_P was calculated as,

$$\Delta R_{3\omega,S} = \frac{R_{3\omega,S} - R_{3\omega,S=0}}{R_{3\omega,S=0}}, \qquad \text{(A. 1)}$$

where $R_{3\omega,S}$ and $R_{3\omega,S=0}$ are the third harmonic resistances for a difference in the Seebeck coefficient $S = S_S - S_P$ and $S = 0$, respectively. This increase is plotted figure A2 for both samples studied in this work. Considering a difference in the Seebeck coefficient between the Ru of the thin films ($S_S = -1.4$ μV K^{-1}), and the Ni of the probe ($S_P = -19.5$ μV K^{-1}) of $S = 18.1$ μV K^{-1} [26], we can expect the error introduced in $R_{3\omega}$ for neglecting thermoelectric effects to not exceed 1% in any configuration and measuring pitch for both samples.

ORCID iDs

Braulio Beltrán-Pitarch https://orcid.org/0000-0002-4596-9582
Benny Guralnik https://orcid.org/0000-0003-3095-3868
Nini Pryds https://orcid.org/0000-0002-5718-7924

References

[1] Ahn W, Shin S H, Jiang C, Jiang H, Wahab M A and Alam M A 2018 Integrated modeling of self-heating of confined geometry (FinFET, NWFET, and NSHFET) transistors and its implications for the reliability of sub-20 nm modern integrated circuits *Microelectron. Reliab.* **81** 262–73
[2] Cai L, Chen W, Du G, Zhang X and Liu X 2018 Layout design correlated with self-heating effect in stacked nanosheet transistors *IEEE Trans. Electron Devices* **65** 2647–53
[3] McPherson J W 2006 Reliability challenges for 45nm and beyond *Proc.—Des. Autom. Conf.* (https://doi.org/10.1145/1146909.1146959)
[4] Adelmann C 2019 On the extraction of resistivity and area of nanoscale interconnect lines by temperature-dependent resistance measurements *Solid State Electron.* **152** 72–80
[5] Von Glasow A, Fischer A H and Steinlesberger G 2003 Using the temperature coefficient of the resistance (TCR) as early reliability indicator for stressvoiding risks in Cu interconnects *IEEE Int. Reliab. Phys. Symp. Proc.* (https://doi.org/10.1109/RELPHY.2003.1197732)
[6] Abdul Wahab M Z, Mamat H and Jalar A 2011 Temperature Coefficient of Resistance (TCR) measurement method to evaluate metal process of CMOS technology *Adv. Mater. Res.* 146–7 1937–40
[7] Schafft H A and Suehle J S 1992 The measurement, use and interpretation of the temperature coefficient of resistance of metallizations *Solid State Electron.* **35** 403–10
[8] Uhlir A 1955 The potentials of infinite systems of sources and numerical solutions of problems in semiconductor engineering *Bell Syst. Tech. J.* **34** 105–28
[9] Thorsteinsson S, Wang F, Petersen D H, Hansen T M, Kjær D, Lin R, Kim J-Y, Nielsen P F and Hansen O 2009 Accurate micro four-point probe sheet resistance measurements on small samples *Rev. Sci. Instrum.* **80** 13710
[10] Petersen D H, Hansen O, Lin R and Nielsen P F 2008 Micro-four-point probe Hall effect measurement method *J. Appl. Phys.* **104** 013710
[11] Witthøft M-L, Østerberg F W, Bogdanowicz J, Lin R, Henrichsen H H, Hansen O and Petersen D H 2018 A variable probe pitch micro-Hall effect method *Beilstein J. Nanotechnol.* **9** 2032–9
[12] Worledge D C and Trouilloud P L 2003 Magnetoresistance measurement of unpatterned magnetic tunnel junction wafers by current-in-plane tunneling *Appl. Phys. Lett.* **83** 84–86
[13] Cagliani A, Østerberg F W, Hansen O, Shiv L, Nielsen P F and Petersen D H 2017 Breakthrough in current-in-plane tunneling measurement precision by application of multi-variable fitting algorithm *Rev. Sci. Instrum.* **88** 095005
[14] Marangoni T A, Guralnik B, Borup K A, Hansen O and Petersen D H 2021 Determination of the temperature coefficient of resistance from micro four-point probe measurements *J. Appl. Phys.* **129** 165105
[15] Guralnik B *et al* 2022 Determination of thermoelectric properties from micro four-point probe *Meas. Sci. Technol.* **33** 125001
[16] Lamba N, Guralnik B, Beltrán-Pitarch B, Rosendal V, Pryds N, Hansen O and Petersen D H 2024 Deconvolution of heat sources for application in thermoelectric micro four-point probe measurements *Int. J. Therm. Sci.* **196** 108716
[17] Beltrán-Pitarch B, Guralnik B, Lamba N, Stilling-Andersen A R, Nørregaard L, Hansen T M, Hansen O, Pryds N, Nielsen P F and Petersen D H 2023 Determination of thermal diffusivity of thermoelectric materials using a micro four-point probe method *Mater. Today Phys.* **31** 100963
[18] Guralnik B *et al* 2021 3ω correction method for eliminating resistance measurement error due to Joule heating *Rev. Sci. Instrum.* **92** 094711
[19] Devanathan V 2021 The Wiedemann-Franz law for electrical and thermal conduction in metals
[20] Wen L G *et al* 2016 Atomic layer deposition of ruthenium with TiN interface for sub-10 nm advanced interconnects beyond copper *ACS Appl. Mater. Interfaces* **8** 26119–25
[21] Popovici M *et al* 2017 Atomic layer deposition of ruthenium thin films from (ethylbenzyl) (1-Ethyl-1,4-cyclohexadienyl) Ru: process characteristics, surface chemistry, and film properties *Chem. Mater.* **29** 4654–66
[22] Deng S, Xiao C, Yuan J, Ma D, Li J, Yang N and He H 2019 Thermal boundary resistance measurement and analysis across SiC/SiO_2 interface *Appl. Phys. Lett.* **115** 101603
[23] Tellier C and Tosser A 1982 Size effects in thin films (https://doi.org/10.1016/c2009-0-12632-6)
[24] Steinmann P, Jacobsen S M and Higgins R 2000 Controlling the TCR of thin film resistors *Eur. Solid-State Device Res. Conf.* (https://doi.org/10.1109/ESSDERC.2000.194812)
[25] Beltrán-Pitarch B, Prado-Gonjal J, Powell A V and García-Cañadas J 2019 Experimental conditions required for accurate measurements of electrical resistivity, thermal conductivity, and dimensionless figure of merit (ZT) using Harman and impedance spectroscopy methods *J. Appl. Phys.* **125** 025111
[26] Burkov A and Vedernikov M 1995 Thermoelectric properties of metallic materials *CRC Handbook of Thermoelectrics* (Routledge) (https://doi.org/10.1201/9781420049718.ch32)